Murine LC3 as a marker of autophagy

Recently, intracellular processing of rat LC3 has emerged as a reliable marker of autophagic activity (1). To ensure that murine LC3 is targeted similarly, we performed double-labeling immunofluorescence studies to track murine LC3 (mLC3) and GFP-fused rat LC3 (rLC3). C2C12 skeletal myoblasts and neonatal rat cardiomyocytes (NRVM) transfected with constructs expressing GFP-mLC3 manifested diffuse, cytoplasmic GFP fluorescence under nutrient-rich conditions. Following amino acid deprivation, an established trigger of autophagy, myc-tagged mLC3 localized as punctate aggregates, which overlapped with GFP-rLC3 (**Figure 1 Online Data Supplement**).

To track the processing of endogenous LC3, we generated an affinity-purified, rabbit polyclonal anti-LC3 antibody. This antibody detected both the unprocessed (LC3-I) and processed (LC3-II) isoforms in cultured NRVMs. Both amino acid deprivation and exposure to hypoxic conditions triggered processing of endogenous LC3 (**Figures 1-2 Online Data Supplement**).

To test for cardiac autophagy in vivo, mice were fasted for 48h. Throughout this time, animals had free access to water, and they manifested no signs of distress. Short-term nutrient deprivation, an established trigger for autophagy in numerous tissues including heart (1-3), induced dramatic and progressive increases in LC3-II in left ventricular (LV) lysates, indicative of increased autophagic activity (**Figure 3A Online Data Supplement**).

Ultrastructural studies were performed in heart to probe for double membrane-bound autophagic vacuoles, a long-established analytical “gold standard” for autophagy. Following short-term nutrient deprivation, significant numbers of both early (containing morphologically intact cytoplasm) and late (containing partially degraded but identifiable cytoplasmic material) (4) autophagosomes and autolysosomes were detected in cardiac myocytes (**Figure 3B Online Data Supplement**). Together, these data demonstrate that cardiac myocyte autophagy is triggered by stress in vitro and in vivo, consistent with prior studies (5), and they establish mLC3 processing and translocation as *bona fide* markers of autophagic activity in cardiac muscle.

Table I: Online Data Supplement

	Sham			sTAB		
	WT	***αMHC-GFP-LC3***	***αMHC-GFP-LC3 x beclin 1$^{+/-}$***	**WT**	***αMHC-GFP-LC3***	***αMHC-GFP-LC3 x beclin 1$^{+/-}$***
Echocardiographic Data						
Heart rate	612±27	690±33	640±35	617±57	585±30	600±49
LVEDD (mm)	1.72±0.04	1.90±0.11	1.90±0.20	3.2±0.2*	3.2±1.0*	2.5±0.5*
LVESD (mm)	0.43±0.08	0.51±0.08	0.50±0.12	2.2±0.07*	2.1±0.9*	1.4±0.6**
%FS	75±6	73±3	74±4	30±2*	31±2*	44±4**
n (animals)	4	6	3	4	5	4
Morphometric and Physiological Data						
BW (g)	25.5±1.3	24.8±0.46	26.1±0.9	24.1±2.0	23.6±1.5	23.8±1.8
HW/BW	4.9±0.3	5.2±0.1	4.7±0.1	9.3±1.2*	9.2±1.7*	9.9±1.6*
LW (mg)	154±11	144±10	154±14	420±80*	450±38*	477±39*
SBP (mmHg)	136±8	134±16	131±4	N/A	N/A	N/A
n (animals)	7	6	3	5	5	4

N/A: not available
* denotes $p<0.05$ vs WT Sham
** denotes $p<0.05$ vs WT sTAB

1. Mizushima, N., Yamamoto, A., Matsui, M., Yoshimori, T., and Ohsumi, Y. 2004. In vivo analysis of autophagy in response to nutrient starvation using transgenic mice expressing a fluorescent autophagosome marker. *Mol Biol Cell* 15:1101-1111.

2. Kuma, A., Hatano, M., Matsui, M., Yamamoto, A., Nakaya, H., Yoshimori, T., Ohsumi, Y., Tokuhisa, T., and Mizushima, N. 2004. The role of autophagy during the early neonatal starvation period. *Nature* 432:1032-1036.

3. Pattingre, S., Tassa, A., Qu, X., Garuti, R., Liang, X.H., Mizushima, N., Packer, M., Schneider, M.D., and Levine, B. 2005. Bcl-2 antiapoptotic proteins inhibit beclin-1-dependent autophagy. *Cell* 122:927-933.

4. Kostin, S., Pool, L., Elsasser, A., Hein, S., Drexler, H.C., Arnon, E., Hayakawa, Y., Zimmermann, R., Bauer, E., Klovekorn, W.P., et al. 2003. Myocytes die by multiple mechanisms in failing human hearts. *Circ Res* 92:715-724.

5. Klionsky, D.J., and Emr, S.D. 2000. Autophagy as a regulated pathway of cellular degradation. *Science* 290:1717-1721.

Figure Legends

Figure 1 Online Data Supplement. LC3 processing in C2C12 myoblasts and neonatal cardiomyocytes.

Panel A. C2C12 cells were co-transfected with GFP-rLC3 and myc-mLC3 and nutrient-deprived for 2 hours. **Left:** GFP signal from tagged rat LC3 aggregates in a punctate pattern, indicative of autophagy. **Middle:** The same cell was labeled by anti-myc primary antibody and cy3-conjugated secondary antibody to detect transfected mLC3. **Right:** Overlay of GFP (rLC3) and cy3 (mLC3) signals demonstrate co-localization of the 2 proteins. Scale bar: 8 μm. **Panel B:** In cultured NRVMs, short-term hypoxia triggered LC3 processing from the cytosolic 18kD LC3-I form to the membrane-bound 16kD LC3-II form. Similar LC3 processing, indicative of increased autophagic activity, was detected in cultured C2C12 skeletal myoblasts (**Panel C**) and NRVM (**Panel D**) subjected to short-term amino acid deprivation (starvation).

Figure 2 Online Data Supplement. Starvation-induced LC3 processing in NRVM.

We developed an affinity-purified polyclonal mouse LC3 antibody. Using this reagent, discrete bands at 18kD and 16kD were detected whose relative abundance shifted with short-term starvation (an established trigger of autophagy), consistent with LC3-I and LC3-II respectively. Depicted here is the entire blot, including LC3-I, LC3-II, and several nonspecific bands.

Figure 3 Online Data Supplement. Starvation-induced cardiomyocyte autophagy *in vivo*.

Panel A. Immunoblot analysis using affinity-purified anti-LC3 reveals an increase in the ratio of processed LC3-II to LC3-I in ventricular lysates isolated from 24h-starved mice compared with control. Mean data from 3 independent experiments. * denotes $p<0.05$ **Panel B.** Ultrastructural features of autophagy are apparent in ventricular cardiomyocytes from 48h-starved mice, including multilamellar vacuoles harboring intracellular contents. Scale bar: 120 nm.

Figure 4 Online Data Supplement. Increased afterload hemodynamic stress, and associated heart failure, does not trigger autophagy in non-cardiac tissues.

Representative immunoblots for LC3 from liver (**Panel A**), kidney (**Panel B**), and brain (**Panel C**) demonstrating that LC3-II/LC3 I ratio is not significantly increased in these tissues following sTAB.

Figure 5 Online Data Supplement: Induction of lysosomal markers was less in *beclin 1*$^{+/-}$ hearts subjected sTAB relative to wild type.

Cathepsin D and LAMP 1 were detected by immunohistochemistry in sTAB ventricle. The abundance of both lysosomal markers was less in *beclin 1*$^{+/-}$ LV post-sTAB (48h) relative to wild type LV post-sTAB. Scale bar: 40 μm.

Figure 6 Online Data Supplement. sTAB-induced pressure-overload heart failure is not associated with declines in body weight.

To test for possible decreases in food intake in heart failure mice, body weight was tracked for 48 hours and compared with animals subjected to short-term food deprivation. Filled squares: sTAB; Open squares: starvation. N=3 in each group.

Figure 7 Online Data Supplement. Fetal gene activation.

RNA dot blots (**Panel A**) reveal increased abundance of ANF mRNA in TAB LV from both WT and Beclin 1 TG hearts. **Panel B**: Mean data quantified from 3 independent experiments. * denotes $p<0.05$ compared with Sham

Supplementary Figure to consider for journal cover. Pressure overload-induced hypertrophy is amplified in Beclin 1 transgenic hearts.

Representative images of hearts from WT and *beclin 1* TG hearts treated as listed. Scale bar: 1 mm.

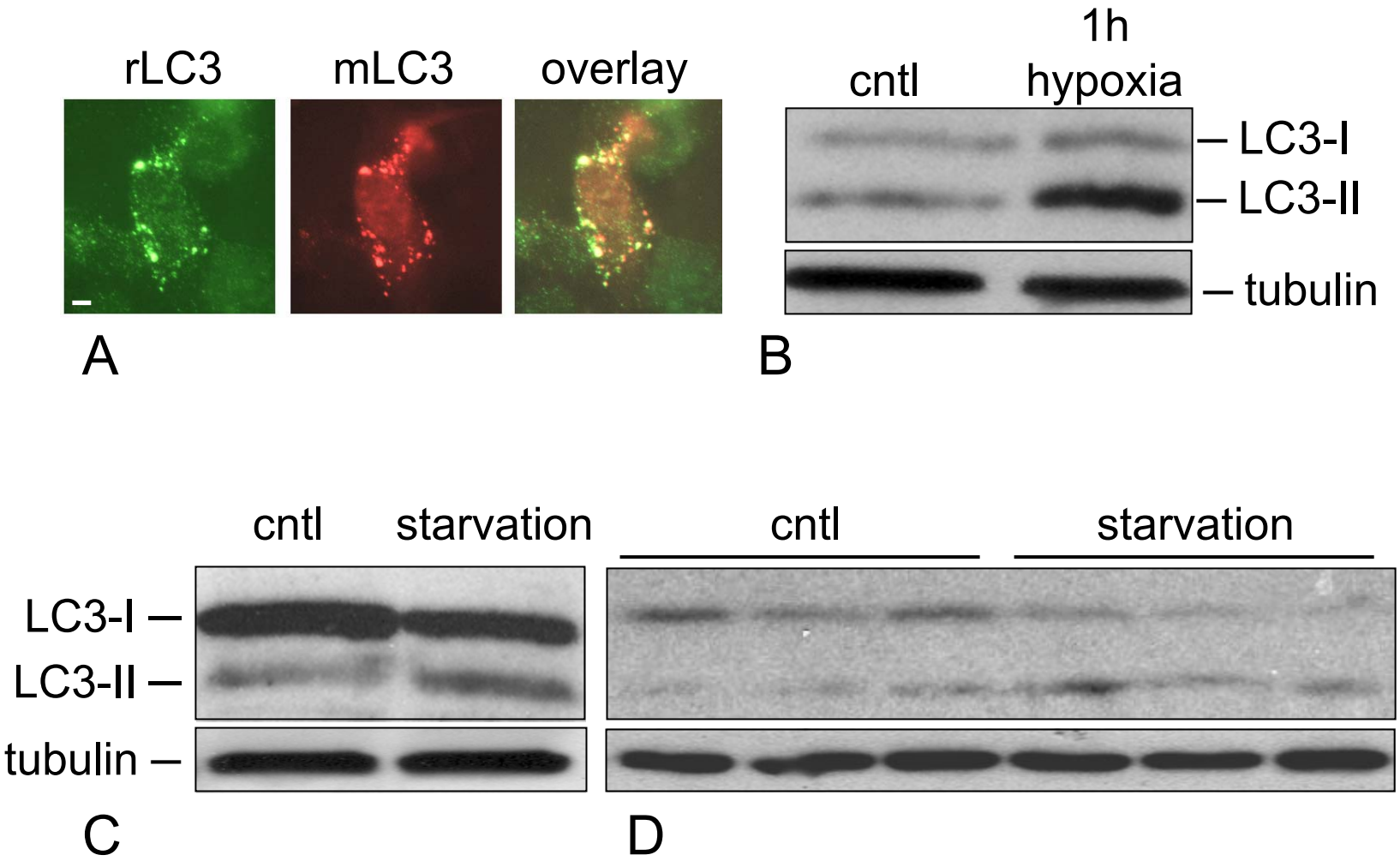

Figure 1 Online Data Supplement

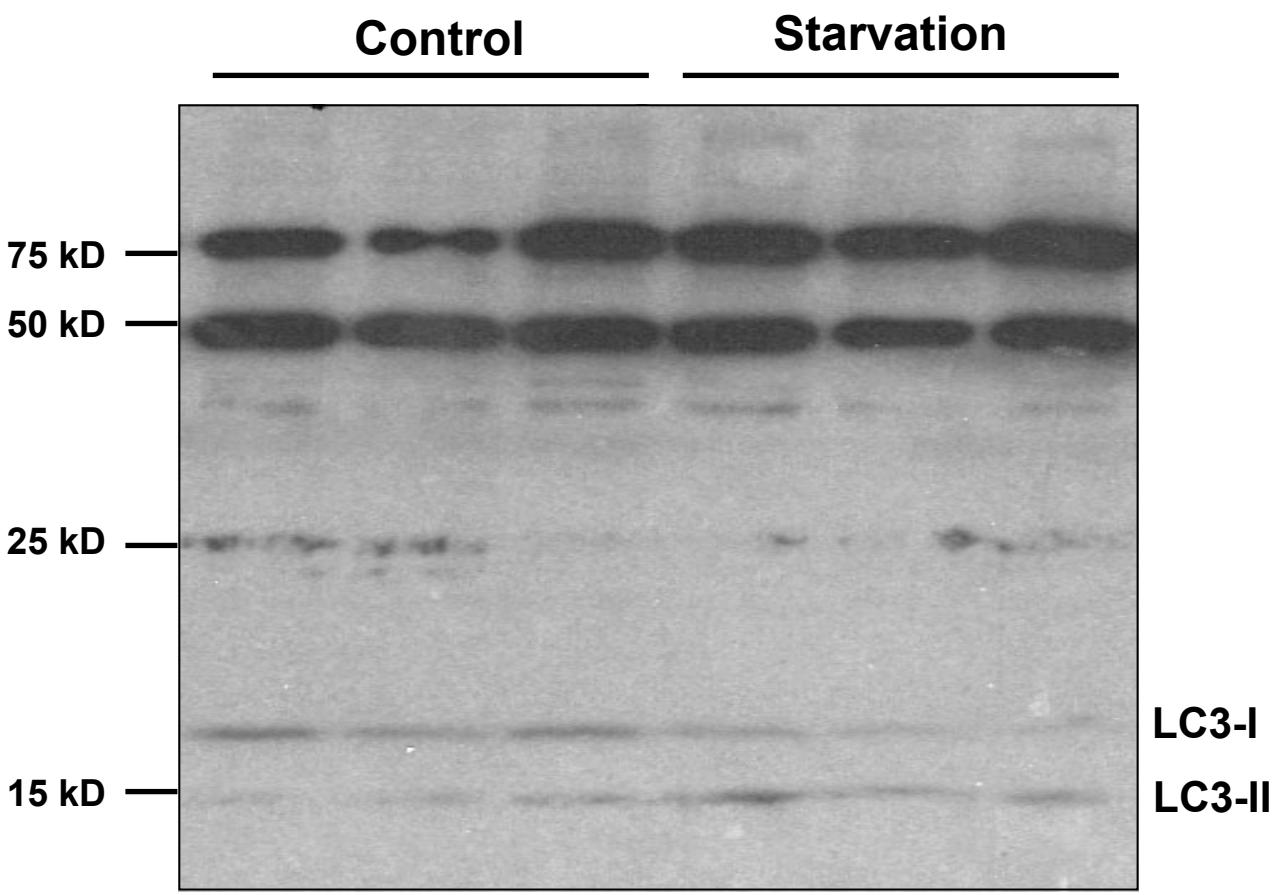

Figure 2 Online Data Supplement

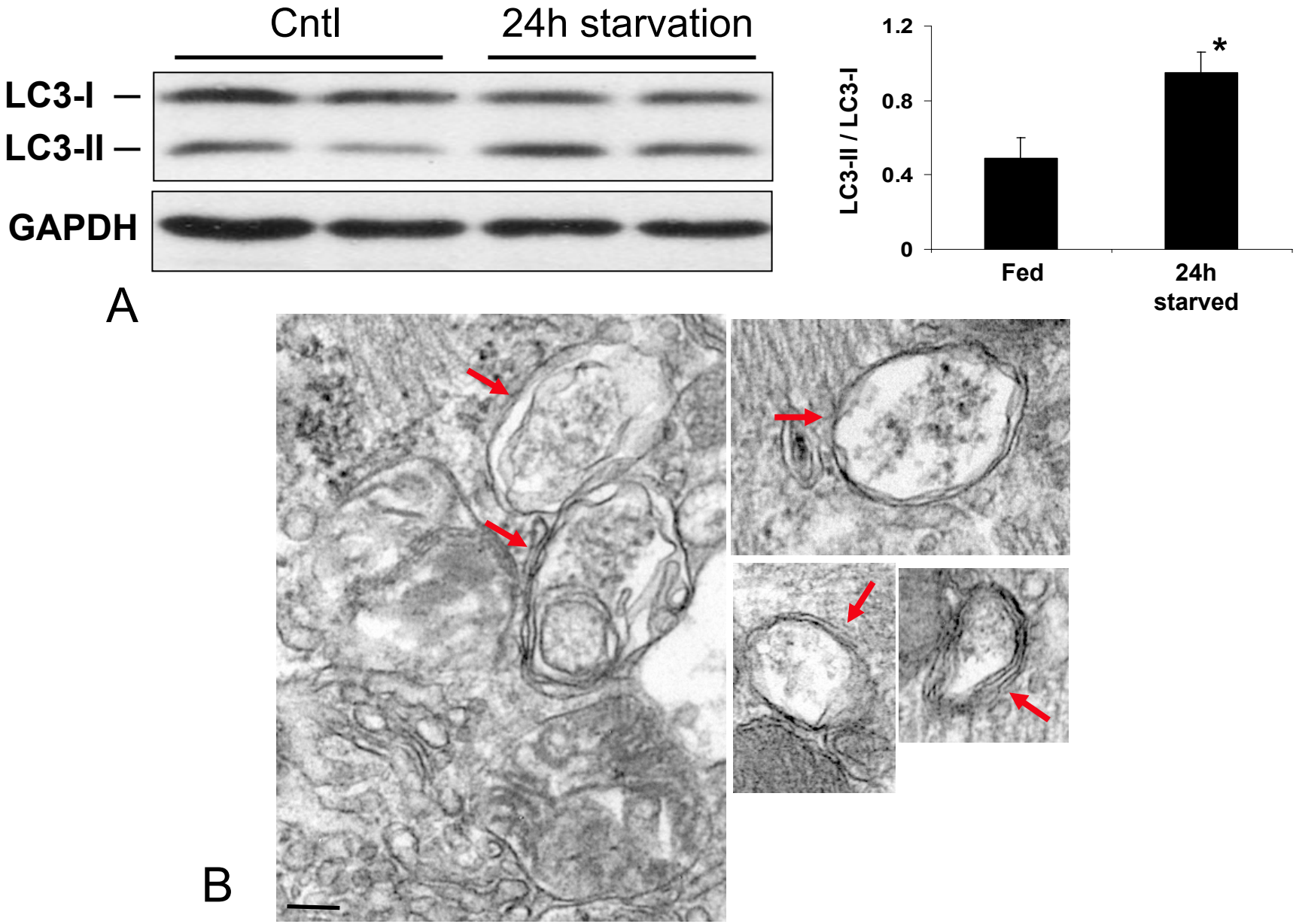

Figure 3 Online Data Supplement

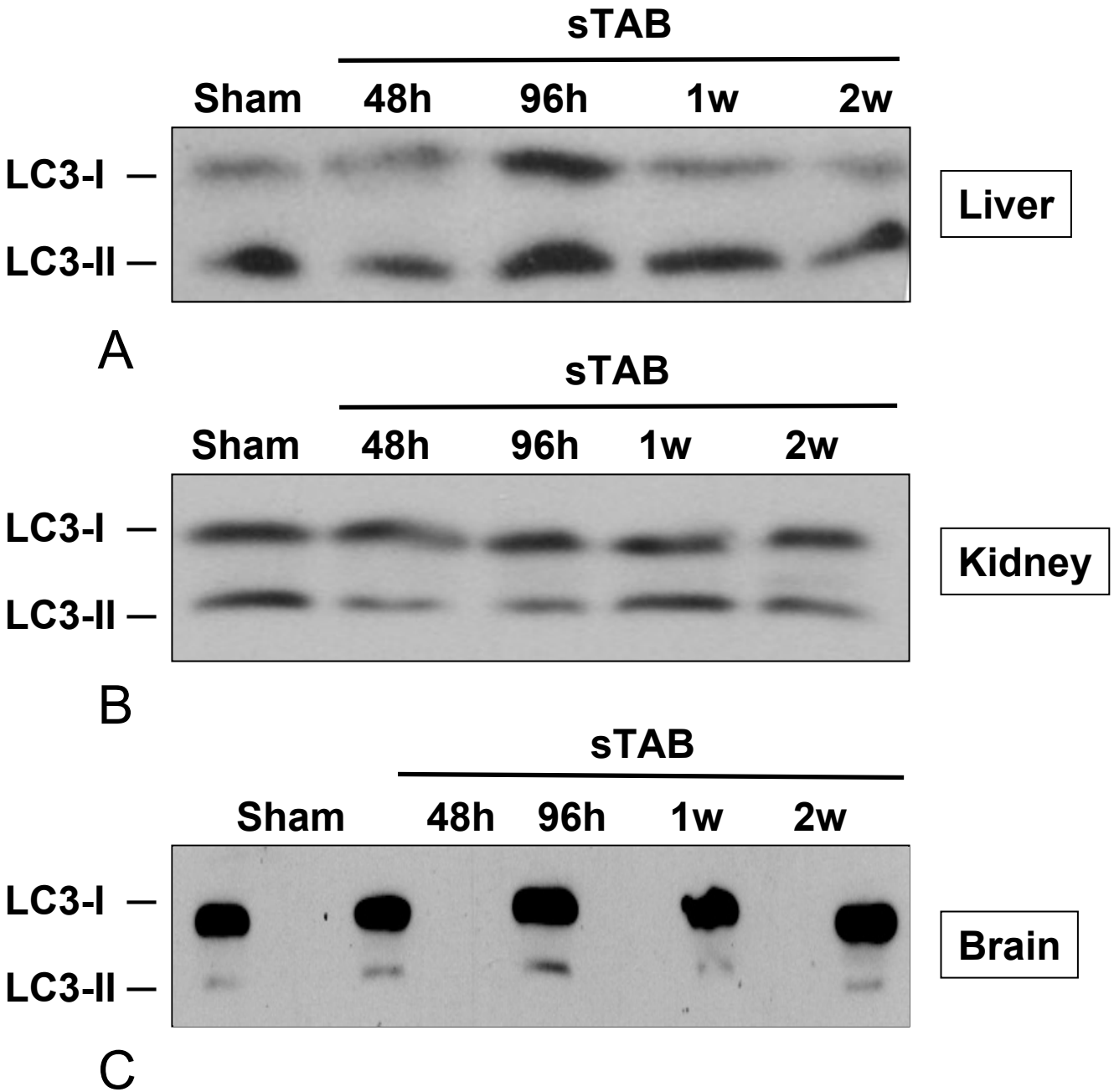

Figure 4 Online Data Supplement

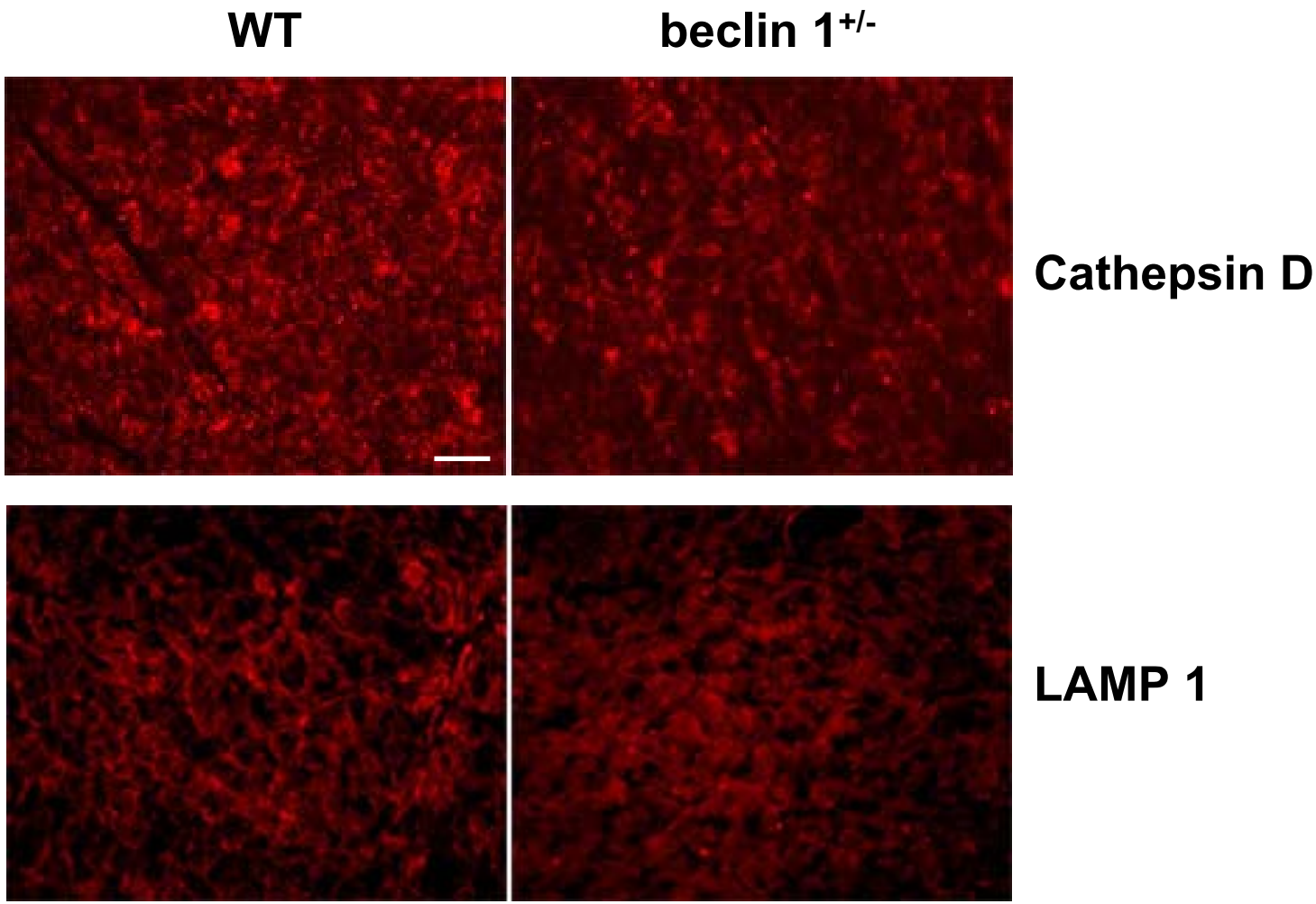

Figure 5 Online Data Supplement

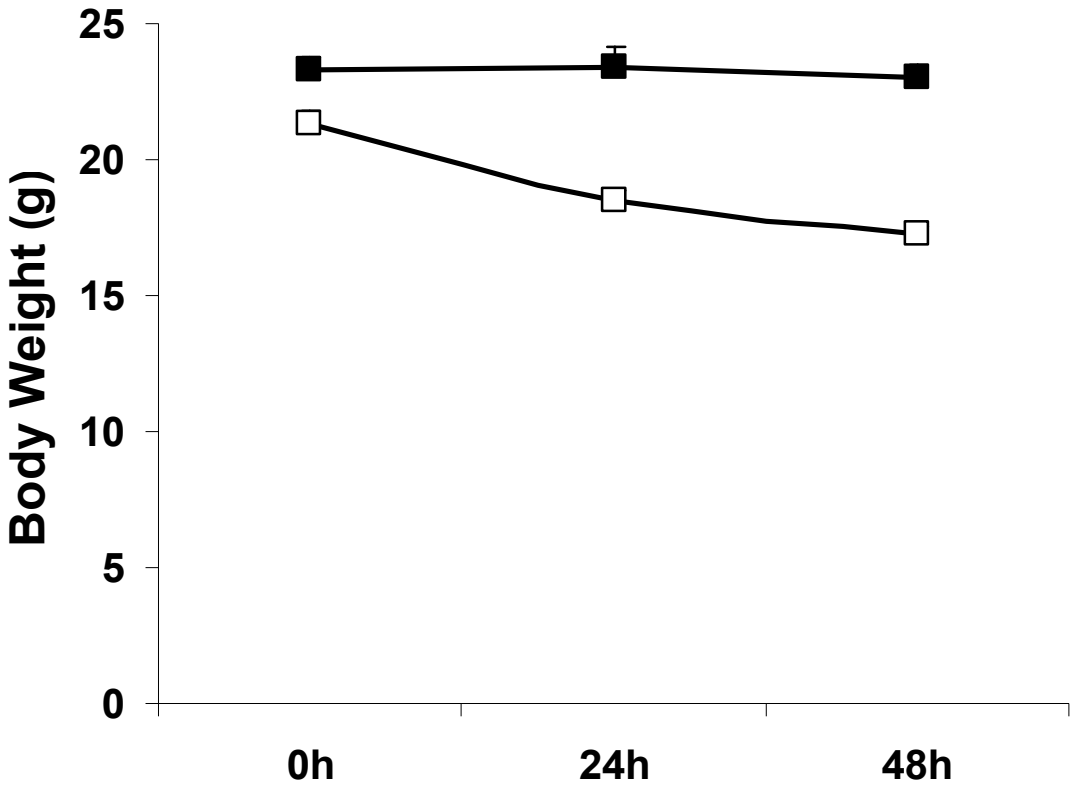

Figure 6 Online Data Supplement

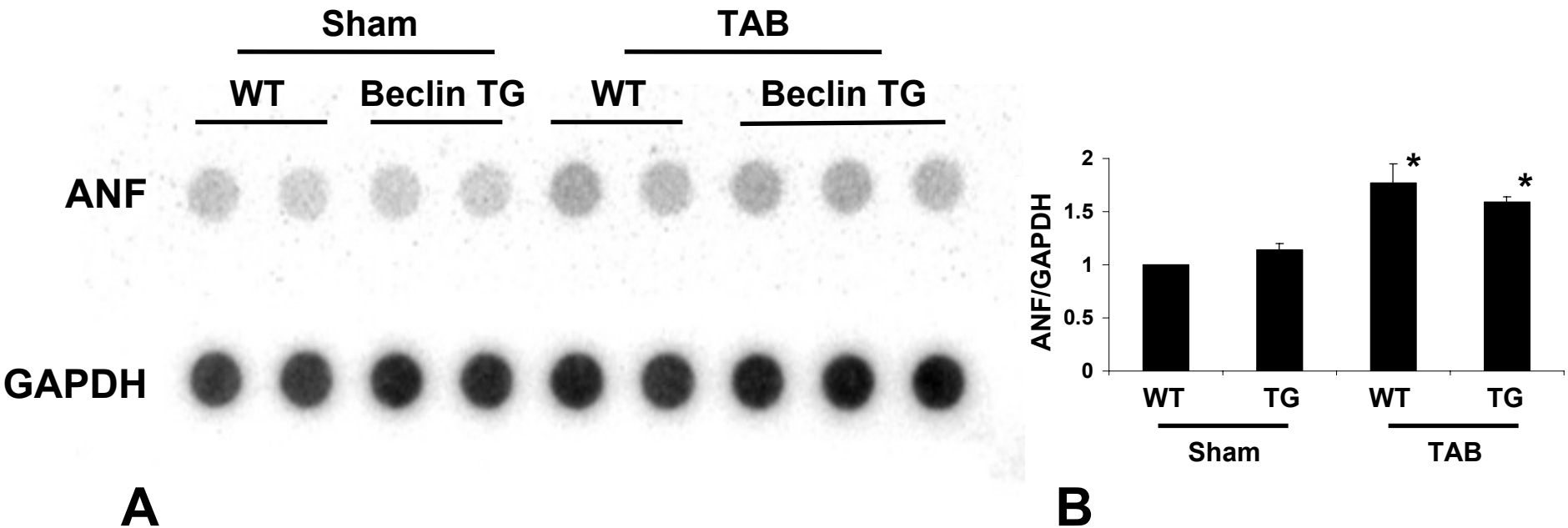

Figure 7 Online Data Supplement